Hydrol. Earth Syst. Sci. Discuss., 5, 2169–2197, 2008
www.hydrol-earth-syst-sci-discuss.net/5/2169/2008/

Hydrology and Earth System Sciences Discussions

Papers published in *Hydrology and Earth System Sciences Discussions* are under open-access review for the journal *Hydrology and Earth System Sciences*

Cost-effective raingauge deployment and rainfall heterogeneity effect on hydrograph simulation in mountainous watersheds

Jr-Chuan Huang[1], Shuh-Ji Kao[1,2], Kang-Tsung Chang[3], Chuan-Yao Lin[1], and Pao-Liang Chang[4]

[1]Research Center for Environmental Changes, Academia Sinica, Taipei, Taiwan
[2]State Key Laboratory of Marine Environmental Science, Xiamen University, Xiamen, China
[3]Kainan University, Taoyuan, Taiwan
[4]Taiwan Central Weather Bureau, Taipei, Taiwan

Received: 2 July 2008 – Accepted: 10 July 2008 – Published: 6 August 2008

Correspondence to: Shuh-Ji Kao (sjkao@gate.sinica.edu.tw)

Published by Copernicus Publications on behalf of the European Geosciences Union.

Abstract

To what extent hydrograph simulation was influenced by the representativeness of rainfall input were examined in meso-scale subtropical mountainous watersheds, accordingly, cost-effective raingauge deployment was suggested. Two nested watersheds in northern Taiwan and two extreme typhoons with torrential rains were undertaken as case studies. The input of radar rainfall estimates with high spatial resolution of 1.3 km^2 served as a reference, which was applied onto hydrograph simulation in TOPMODEL. After calibration, optimal parameters were obtained and fixed to examine effect of deviated rainfall on hydrograph. To mimic possible raingauge networks we designed four raingauge number classes: very low (3 points/total pixels), low (10 points/total), medium (20 points/total), and high (50 points/total) based on radar rainfall for the two watersheds in different size, thus, creating wide spectrum of raingauge density. All the corresponding hydrographs were compared with the reference hydrograph to probe errors in event discharge induced by calculated rainfall input.

Results showed that with the decreasing of raingauge density the biases (indicated by RMSE) of rainfall field estimates increase and the potential variability in rainfall field due to random sampling in raingauge location is exaggerated. By contrast, biases in model hydrographs are significantly smaller than that in rainfall field. When the raingauge governing area is <10 km^2/gauge, the biased rainfall field shows no detectable effect on hydrographs. Incomparably lower RMSE in hydrograph indicates that surplus and deficit rainfalls at different locations were compensated in model simulation. In term of reliable hydrograph simulation, obviously, the criterion for raingauge density is not as high as that for rainfall estimate. When gauge governing is <20 km^2/gauge, both the rainfall and discharge were successfully (±10% error) estimated in term of total volume. Accordingly, we suggested that covering area ~20 km^2/gauge is acceptable for raingauge deployment to constrain the inherent variability in rainfall field and hydrograph simulation in mountainous watersheds.

1 Introduction

Accurate runoff simulation for flood forecasting, mitigation and water resource management relies on accurate rainfall monitoring over spatiotemporal variability (Singh, 1997; Bell and Moore, 2000), which is the major forcing for runoff variability within a catchment. However, interactions between meteorological conditions and geomorphologic factors (Creutin et al., 1997) complicate the rainfall variability. Traditionally, hydrologists use a rainfall field interpolated from limited point rainfall measurements or even scarce points by assuming a homogeneous rainfall field to simulate discharges. Many of those studies showed that simulations can reach 0.7∼0.9 of efficiency coefficient (hereafter EC, which is proposed by Nash and Sutcliffe, 1970). Unsatisfactory performances or unexpected contradictions in simulated hydrographs are generally attributed to the insufficiency of rainfall input.

Since the 1990s, radar techniques have been used to estimate spatiotemporal rainfall patterns and rainfall forecast (Krajewski and Smith, 2002). Despite of technique problems, such as ground clutter, anomalous propagation and hail, etc. (Terblanche et al., 2001), major benefits of radar observations include estimations in large areas, though indirect, and high spatiotemporal resolution. In addition, radar rainfall forecasting has shown to be more reliable and satisfactory than that by even dense raingauge networks (Wu et al., 2007; Chen et al., 2006). Interestingly, when radar rainfall was applied onto many hydrograph simulations (Syed et al., 2003; Celleri et al., 2007), similar performances were obtained as those by limited raingauge data. This similar performance draws our attention to the inter-play of rainfall variability, estimated rainfall field and raingauge density on hydrograph simulation.

How many raingauges can represent the rainfall field and generate reliable hydrograph is especially important for model in meso-scale mountainous catchments in Taiwan. Taiwan locates on the typhoon alley that generally 3–5 typhoons (tropical cyclone) invade every year bringing torrential rainfall within 1–2 days. To benefit near-real-time flood warning system and optimal reservoir operation, the Central Weather Bureau

(CWB) in Taiwan installed four radars covering almost entire Taiwan to provide high spatial (1.3 km^2) and temporal (10 min) resolution rainfall estimate for management application. Weather radar is calibrated by using gauged rainfall. Such combination offers us great opportunity to probe the raingauge density effect on hydrograph simulation in rugged mountainous region.

This study aimed to determine the minimum raingauge density, thus cost-effectively, that required representing the rainfall input for hydrograph simulation in meso-scale subtropical watersheds. Two sub-watersheds with drainage areas of 622 km^2 and 116 km^2 in northern Taiwan are applied. Hourly radar rainfall estimates during two typhoon events are used as "true" rainfall fields. We randomly selected data points out of the true rainfall to mimic raingauge networks with different density. Through such stochastic experiment we examined errors derived from biased rainfall field by comparing the simulated hydrographs with the reference hydrograph derived from "true" rainfall. The effects of biased rainfall on model hydrographs are presented and discussed.

2 Material and methods

2.1 Study site

The locations of the four radars and the coverage of radar rainfall estimates are shown in Fig. 1a. A nested watershed at upstream Shih-Men Reservoir was chosen as the study site (Fig. 1b). This reservoir is a major water conservancy facility for agricultural irrigation, hydropower generation, public water supply, and flood prevention for northern Taiwan region. The nested watershed includes the subwatersheds of the Xia-Yun and Xiu-Luan. The Xia-Yun with a drainage area of 622 km^2 originates from Pin-Tian Mt. (3529 m a.s.l.), and the Xiu-Luan with a drainage area of 116 km^2 has its source in Da-Ba-Jian Mt. (3459 m a.s.l.). The North Region Water Resources Office of Water Resources Agency (WRA) maintains 10 raingauges and two discharge stations in the

study area.

Lithologic formations are mainly composed of sandstone, shale, and slate (Taiwan Central Geological Survey, 2000) and the soil type is mainly Lithosols (Entisols). Nearly 87% of this study area is covered by forest. The mean annual temperature is 21°C, with a mean monthly temperature of 27.5°C in July and 14.2°C in January. The annual precipitation averages 2370 mm. Typhoons in summer and the northeast monsoon in winter are two dominant contributors of precipitation in this area. About 75% of the annual precipitation occurs in the typhoon season from May to September. Consequently, the discharges in these two subwatersheds are significantly different during the wet and dry seasons. The mean daily discharge is 36.9 cm in the Xia-Yun and 6.1 cm in the Xiu-Luan. The mean daily discharges are 53.9 and 8.9 cm in the wet season and 19.5 and 3.3 cm in the dry season, for the Xia-Yun and Xiu-Luan, respectively.

2.2 Typhoon events

Matsa and Korsa are two recent typhoons that caused dramatic surge of discharge in the two watersheds. Typhoon Matsa (3–6 August 2005) crossed the northern tip of Taiwan in a SE-NW direction. During its peak intensity on 4 August, Typhoon Matsa had a 250-km storm radius with a low pressure reading of 965 hPa and the maximum wind speed up to 45 m s^{-1}. The track of Korsa (4–7 October 2007) was similar to Matsa but much closer to Taiwan. During its peak intensity, Typhoon Korsa had a low pressure reading of 935 hPa and maximum wind speed to 58 m s^{-1}. Nine people were killed by this typhoon and the estimated total loss in agriculture is 142.3 million USD.

Table 1 shows the basic attributes of rainfall and runoff in the Xia-Yun and Xiu-Luan during the typhoons. The rainfall attributes derived from radar rainfall include total rainfall, duration, average rainfall intensity, and maximum rainfall intensity. We compared the radar rainfall with the 10 raingauges within the watershed on hourly basis; the correlation coefficient is as high as 0.6–0.9 indicating the capability of radar in hourly rainfall estimation. In term of total rainfall, we found Xia-Yun and Xiu-Luan received significantly different total rainfall by ~220 mm during the Matsa invasion period (Table 1)

although the two watersheds are nested closely. Compared to Korsa, larger total rainfall RMSE values of Matsa (Table 1) also supports the rainfall heterogeneity in Matsa is larger within watershed. Rainfall caused by typhoon can be quite variable in space.

2.3 Hydrologic model description

This study used a modified TOPMODEL (Beven and Kirkby, 1979; Huang et al., 2007). Following many hydrologic models, TOPMODEL assumes that rainfall can keep on the surface only when it exceeds the root zone capacity. Therefore, two parameters called maximum root zone storage ($S_{r\,\max}$) and root zone storage (S_r) are used to characterize the rainfall retention and interception. The surface raindrop, either infiltrating to the subsurface or forming the surface runoff, depends on the reduced moisture deficit per unit volume of soil from saturation (D_i). Note that Walter et al. (2002) suggested replacing soil moisture deficit by using reduced moisture deficit owing to better interpretation and improved modeling performance in arid or semiarid environment and in cases of rain storms with high rainfall intensity. The surface runoff can be estimated by the empirical formula (Liu et al., 2003):

$$Q_{\mathrm{sur},i} = RC_i \cdot (1 - D_i)^{\alpha} \tag{1}$$

where $Q_{\mathrm{sur},i}$ is the surface flow in the cell, and RC_i is the runoff coefficient (0~1.0) and can be estimated by land use type. For example, the impervious surface having a higher value (closer to 1.0) means that all surface raindrop will form the surface runoff. The parameter α, representing the proportion of surface flow in different soil moisture conditions, can also be estimated by land use and soil type.

For surface flow, the unit response function composed by the network width function and hydrodynamics is used to represent the surface flow. Here we use the approximate solution derived from the diffusive transport approach proposed by Liu et al. (2003).

The approximate solution is

$$U(t) = \frac{1}{\sigma\sqrt{2\pi \cdot t^3/t_0^3}} \exp\left[-\frac{(t-t_0)^2}{2\sigma^2 t/t_0}\right] \quad (2)$$

where $U(t)$ [$1/T$] is the flow path unit response function, t_0 [T] is the average travel time of the cell to outlet along flow path, and σ [T] is the standard deviation of the flow time. The t_0 and σ are spatially distributed parameters both of which are retrieved from DEMs (40 m resolution). Accordingly, each flow path has different parameters depending on the length of the flow path and the physical characteristics of the flow path element. In our model, Mannings' surface roughness, n, is embedded implicitly in the above equation. The total surface flow hydrograph at the watershed outlet is obtained by a convolution integral of the flow response from all grid cells. Because each cell has its own travel time and the standard deviation of travel time, this routing method does consider rainfall spatial variability by allowing each cell to have different temporal rainfall time series and changes of the discharge response to rainfall.

For the subsurface flow, this study used the TOPMODEL routing scheme. Given the exponential transmissivity assumption, the local reduced moisture deficit can be estimated by:

$$D_i = \overline{D} + m\left[\gamma - \ln(a_i/T_0 \tan\beta_i)\right] \quad (3)$$

where $\overline{D}$ is the mean value of the reduced moisture deficit over the entire catchment and γ is the mean value of the topographic index, $\ln(a/T_0 \tan\beta)$, over the catchment area. The parameter T_0 in the topographic index is the lateral transmissivity as the soil is saturated [L^2/T], a is the specific contributing area defined as the drainage area per unit contour length [L], and $\tan\beta$ is local gradient [−]. Both a and $\tan\beta$ can be derived directly from DEMs through terrain analysis. Based on Eq. (3) and the exponential transmissivity assumption, the subsurface runoff can be estimated by the recession

curve function:

$$Q_{sub} = A \cdot e^{-\gamma} \cdot e^{-\overline{D}/m} \quad (4)$$

Given rainfall time series, Eqs. (1) and (3) can simulate the surface and subsurface flows for each time step. Accordingly, 7 parameters, namely $S_{r\,max}$, S_r, n, RC, α, m, and T_0, are needed to route the model.

Since this study focuses on the influence of rainfall spatial variability, to reduce the complexity of parameter estimation or calibration (Beven, 2001), we assumed all 7 parameter are homogeneous over the whole catchment although land use, soil and topographic properties within the catchment can be planted in the model.

2.4 Experimental design

A random sampling procedure was adopted. First, we designed four classes of raingauge number: very low (3 points/total pixels), low (10 points/total), medium (20 points/total), and high (50 points/total). Points are randomly sampled and 50 sets were created for each class to represent possible raingauge networks. Since the total area of the two studied watersheds are different, this random sampling generates a high spectrum of raingauge density. Once the points were selected, the Thiessen's polygon was used to interpolate the spatial rainfall pattern.

As mentioned earlier, this study tries to determine the representativeness of each sample set, thus, the deviations between the sample set and radar rainfall were calculated by using amount ratio (total rainfall derived from sample set over total rainfall derived from radar rainfall) and RMSE (root mean square error). The RMSE was calculated as:

$$\mathrm{RMSE} = \frac{\sum_{t=0}^{T} \sqrt{\frac{\sum_{i=1}^{n} (R_{e,i} - R_{r,i})^2}{n}}}{T} \quad (5)$$

where $R_{e,i}$ is the rainfall estimate derived from the specific sample set, $R_{r,i}$ is the radar rainfall estimate at the same pixel, n is the total grid number, and T is the total time step. The amount ratio indicates the accuracy in amount and RMSE shows the variability between sample set and radar rainfall.

In this study, we used radar rainfall to calibrate the seven parameters and to obtain the "reference hydrograph" in model output. The reference hydrograph was taken as standard for comparisons because the observed discharge might include some unknown errors. All simulations derived from those sets of various gauge numbers were compared to evaluate the effect of rainfall input on performance of hydrograph simulation under conditions of fixed parameter set. Thus the effect of biased rainfall input on hydrograph simulation can be quantified. Similarly, the amount ratio and RMSE were also used in comparisons of discharge amount and hydrograph.

2.5 Transform the point density to covering area

Our experimental design applies four classes of fixed number of sampling point in total radar pixels. Since the radar data has larger coverage than watershed; thus, sometimes the sampled point appears outside of the watershed. Only when selected points are effective in rainfall contribution according to Thiessen's polygon interpolation, we considered them as effective raingauges for gauge number calculation. Thus the total number of sampled points in each set may not be a precise value as we define originally.

On the other hand, the two watersheds are in different size (i.e. different in total pixel); accordingly, above sampling procedure generates a wide range of raingauge density. In Xia-Yun, the means of raingauge number are 2.8 (2–3), 8.5 (6–10), 15.3 (11–19), and 31.6 (27–38), which are corresponding to covering areas (watershed area over raingauge number) of 207.3, 73.0, 40.7, and 19.7 km^2/gauge, respectively, for the four sampling classes. In Xiu-Luan, the means of raingauge number are 2.9 (2–3), 8.6 (7–10), 15.0 (12–18), and 30.9 (24–37) and the covering area are 39.5, 13.4, 7.8, and 3.8 km^2/gauge, respectively. Such a transformation from point density to covering area

benefits our discussion and conceptually useful in management.

3 Results and discussion

3.1 Reference hydrograph

Based on 10 000 trials in parameter combination (Huang et al., 2006) and EC for performance criterion, the calibrated parameter set for Xia-Yun are: $S_{r\,max}$=25.4 mm, S_0=14.0 mm, n=0.114, RC=0.32, α=1.9, m=15.3, and T_0=11.6 m^2/h and the parameter set for Xiu-Luan are: $S_{r\,max}$=10.2 mm, S_0=9.9 mm, n=0.184, RC=0.59, α=1.9, m=10.3, and T_0=6.8 m^2/h. Compared to the observed discharges in Xia-Yun, EC values are 0.86 and 0.88 during Matsa and Korsa, respectively (Fig. 2a, b). In Xiu-Luan, they are 0.92 and 0.88, respectively, for Matsa and Korsa (Fig. 2c, d).

In Xia-Yun, the total simulated runoff is 461 mm for Matsa and 458 mm for Korsa. In Xiu-Luan, the total simulated discharge is 547 mm for Matsa and 360 mm for Korsa (Note that we use runoff depth for comparison with rainfall). Compared to observations, the total water discharges were simulated well except the case during Masta at Xia-Yun with 20% lower in total discharge. The reason for the underestimations might come from model structure error, imperfect descriptions of input data for landuse and soils. Regardless the possible errors and their causes, the simulated hydrographs were taken as reference with respect to our purpose. Overall speaking, our reference hydrographs fitted well with observations.

3.2 Biased rainfall input, hydrograph output and raingauge density

The estimated total amounts of rainfall and discharge of individual density class were presented (Tables 2, 3) to illustrate the effect of biased rainfall data on the total amount of rainfall and discharge. In Table 2, the ranges of averages of total for rainfall in the four classes are 660–670 mm, 636–642 mm in Xia-Yun during typhoon Matsa (radar rain-

fall: 661 mm) and Korsa (radar rainfall: 640 mm), respectively. And the ranges for the four classes in Xiu-Luan during Matsa (radar rainfall: 881 mm) and Korsa (radar rainfall: 621 mm) are 840–878 mm and 622–625, respectively. Compared to the respective radar total rainfall (Table 1), those average values are comparable and affected little by changing raingauge density. However, the standard deviations for total rainfall decreased sharply with the increase of gauge number. No doubt, limited raingauges result in greater deviation in estimating total rainfall. As mentioned earlier, the inherent rainfall heterogeneity during Matsa is larger; again, we can see sampling-induced fluctuation in total rainfall estimate is larger at the same gauge density level in the Matsa case when comparing with that in Korsa (Table 2).

For total discharges, similarly, the averages of total discharge are affected little by raingauge density; yet, the deviation is much larger in low density condition. Here we made a scatter plot by using R_{set}/R_{radar} (R_{set} and R_{radar} indicate, respectively, the rainfall amount derived from the sample set and the full radar estimates) in x-axis and Q_{set}/Q_{radar} (Q_{set} and Q_{radar} indicate, respectively, the discharge amount derived from the sampled set and the full radar estimates) in y-axis (Fig. 3) to demonstrate their co-variability. All data points fell close to 1:1 line showing a strong positive correlation. The accurate total discharge can be obtained only by accurate total rainfall estimate. The class with higher raingauge density obviously have more chance to give successful results (more data points fell within the range of 0.95–1.05; points outside this range are not shown).

A good estimate of total amount, however, does not guarantee an accurate estimate in each time step. To reveal the temporal variations of rainfall and discharge and the deviations between radar rainfall and sampled rainfall in each time step, time series data were shown in Figs. 4, 5, 6 and 7 (left panel). We shaded the rainfall range for the 50 sets in each gauge number class. In those plots, shaded zones were found to decrease as the increasing gauge density. Meanwhile, the largest deviation generally appeared during the peak rainfall. Similarly, we could find the similar patterns that the shaded zone decreases as the increasing gauge number and the largest deviation ap-

pears during the peak flow as well (Figs. 4, 5, 6 and 7, right panel). Widened shaded zones, in fact, imply that the rainfall heterogeneity during heavy rainfall periods was relatively larger; the larger rainfall heterogeneity could not be represented well by limited gauges and consequently resulted in the larger biases in peak flow simulations.

Summarized result above, the representativeness of rainfall field was determined by both the natural rainfall spatial variability and gauge density. It also indicated that the increasing gauge number could improve the hydrograph simulation, particular in peak flow.

3.3 Overall residual error caused by biased rainfall

According to above discussion, the residual errors over rainfall spatial variability in peak rainfall may have important influence on peak flow simulation. Compared the rainfall RMSE (hereafter R_{RMSE}) values with the discharge RMSE (hereafter Q_{RMSE}, which represents the simulation performance), we examined the effect of sampling error on hydrograph simulation (Table 4 and Fig. 8). The averages of R_{RMSE} during Matsa and Korsa ranged from 8.59–4.00 mm and 7.80–3.93 mm in Xia-Yun (Table 4). In Xiu-Luan, the averages varied from 5.45–1.91 mm and 4.55–1.90 mm. Meanwhile, the Q_{RMSE} averages in Xia-Yun ranged from 1.75–0.23 mm and 1.13–0.23 mm for Matsa and Korsa, respectively. In Xiu-Luan, the Q_{RMSE} averages varied from 0.83–0.06 mm and 0.33–0.03 mm for Matsa and Korsa, respectively. Both R_{RMSE} and Q_{RMSE} averages showed a sharply decreasing trend with the increasing gauge density. Thus, the residual error or variability could be diminished by increasing gauge density. Interestingly, the average of Q_{RMSE} was much lower than the average of R_{RMSE} throughout all gauge number classes.

The R_{RMSE} and Q_{RMSE} for individual set were plotted together in Fig. 8. Figure 8a and b showed the results in Xia-Yun during Matsa and Korsa, respectively. Figure 8c and d were the results for Xiu-Luan. Compared to the linear correlation in amount ratio shown in the Fig. 3, the co-variability between R_{RMSE} and Q_{RMSE} were quite different not following the 1:1 line. The Q_{RMSE} value increases non-linearly with the increasing

R_{RMSE}. The biases of rainfall field and its potential variability are exaggerated due to random sampling in raingauge location when gauge density was low. However, under low density condition the promising simulations could still be obtained though rainfall input was biased. The hydrograph at watershed outlet is the convolution of rainfall spatial pattern and landscape in time series and thus biases in rainfall field were compensated. This explains why researchers often have good hydrological simulations with limited raingauge data.

3.4 Effective raingauge deployment and pseudo-hydrograph

Based on our experiment results, the criterion for cost-effective raingauge deployment depends on the targets we want to probe. In term of total rainfall and discharge the criterion is the same since they vary proportionally. However, the criterion for obtaining a reliable hydrograph is less strict than that needed for reliable rainfall field estimate. The key issue of raingauge deployment was thus addressed by the cost-effect relationship under the tolerance of error and budget. To identify the relationship, the whole rainfall amount ratio, discharge amount ratio, R_{RMSE}, and Q_{RMSE} were plotted against raingauge density (here for convenience we use covering area per gauge) for discussion (Fig. 9a, b, c, and d). For rainfall amount ratio and discharge amount ratio (Fig. 9a, b), when the covering area is less than 20 km^2 (vertical dashed line in Fig. 9) the error of amount estimate for both rainfall and discharge can be better than ±10% regardless the raingauge locations.

At fixed covering area ~20 km^2/gauge, the upper and lower limit of R_{RMSE} are around 5.0 mm and 3.0 mm, respectively (Fig. 9c). By contrast, the upper bound of Q_{RMSE} is lower than 1 mm and the lower bound is even lower than 0.1 mm. The derivation of R_{RMSE} includes spatial variability, thus, hydrological processes that translate spatiotemporal rainfall into temporal discharge apparently lead to lower Q_{RMSE} due to dimension reduction. Such dimension reduction created a situation that when the covering area ranges 20–100 km^2 we still have good chances to derive correct total rainfall and total discharge. However, based on Fig. 9c we know that those cases with good total

amount estimation hold false rainfall field (i.e. high R_{RMSE}) under lower rainaguge density. Those cases of low Q_{RMSE} (i.e. high performance simulation with Q_{RMSE}<1 mm) at low density raingauge conditions (covering area>20 km^2) is pseudo-hydrograpy since all of those correct hydrographs were derived from seriously biased rainfall. Those pseudo-hydrographs may compromise uncertainty analysis in hydrological simulation.

In fact, Fig. 9c indicates that we can continuously improve the rainfall estimate by increasing raingauge number, however, the improvement in hydrograph simulation is limited when the covering area <10 km^2/gauge (Note that 0.5 of Q_{RMSE} approximates to 0.95 or higher of EC depended on cases). Obviously, when raingauge density reaches such a high density condition, those biases in rainfall field can't alter the hydrograph too much because their contributing area is limited with respect to the whole watershed. Therefore, to get accurate rainfall estimate raingauge density should be as higher as possible. By contrast, covering area of ~20 km^2 was generally proper and cost-effective for hydrograph simulation.

As discussing the effect of biased rainfall on hydrograph simulations, it is fortunate that hydrograph was not that sensitive to the rainfall biases and thus very high spatial resolution of rainfall field is not necessary. Nevertheless, the suggested covering area of 20 km^2 may act as guidance for raingauge networks in hydrograph simulation. This covering area is sufficient and cost-effective to constrain the inherent variability, the crucial factor in flood warning system. Meanwhile, it may also be applied to the resembling environment conditions, such as Mediterranean areas.

4 Conclusion

Proper raingauge network may represent the typhoon-induced rain field, which is a function of rainfall heterogeneity and raingauge number. The former affected by meteorological and geomorphologic conditions is a key player and the latter involved sampling error is the second. Increasing raingauge density is important in diminishing the biases in rainfall estimate. However, as discussing the effect of deviated rainfall field

on hydrograph simulation, it's fortunate that hydrograph can compensate errors in rainfall estimate; therefore, lower raingauge density is needed for successful total water discharge and hydrograph simulation. As the covering area per gauge is <10 km^2, the sampling errors are not detectable in simulated hydrographs because the covering area with respect to the whole watershed is sufficient to resolve a reliable hydrograph. On the other hand, due to the dimension reduction from spatiotemporal rainfall input to temporal hydrograph we may have very good chances to obtain successful hydrographs even raingauge density is low; however, those correct hydrographs are derived from biased rainfall. The pseudo-hydrograph will compromise uncertainty analysis in hydrological simulation.

Acknowledgements. The authors are grateful to Northern Region Water Resources Office, Taiwan Central Weather Bureau, and Water Resources Agency for providing precipitation, radar reflectivity and discharge records. This study is support by Taiwan National Science Council, project number: NSC-96-2628-M-001-028.

References

Bell, V. A. and Moore, R. J.: The sensitivity of catchment runoff models to rainfall dara at different spatial scales, Hydrol. Earth Syst. Sci., 4, 653–667, 2000, http://www.hydrol-earth-syst-sci.net/4/653/2000/.

Beven, K. J. and Kirkby, M. J.: A physically based, variable contributing area model of basin hydrology, Hydrol. Sci. B., 24, 43–69, 1979.

Beven, K. J.: Parameter Estimation and Predictive Uncertainty, in: Rainfall-Runoff Modelling, The Primer, edited by: Beven, K. J., Wiley, New York, pp. 217–253, 2001.

Celleri, R., Willems, P., Buytaert, W., and Feyen, J.: Space-time rainfall variability in the Paute Basin, Ecuadorian Andes, Hydrol. Processes, 21, 3316–3327, 2007.

Chen, C., Lee, W., and Yu, F.: Debris flow hazards and emergency response in Taiwan, in: Monitoring, Simulation, Prevention and Remediation of Dense and Debris Flows, edited by: Lorenzini, G., Brebbia, C. A., and Emmanouloudis, D. E., WIT Press, Southampton, Boston, pp. 311–320, 2006.

Creutin, J. D., Andrieu, H., and Faure, D.: Use of weather radar for the hydrology of a mountainous area. Part II: radar measurement validation, J. Hydrol., 193, 26–44, 1997.
Huang, J. C., Kao, S. J., Hsu, M. L., and Lin, J. C.: Stochastic procedure to extract and to integrate landslide susceptibility maps: an example of mountainous watershed in Taiwan, Nat. Hazards Earth Syst. Sci., 6, 803–815, 2006, http://www.nat-hazards-earth-syst-sci.net/6/803/2006/.
Huang, J. C. and Kao, S. J.: Typhoon-induced storm hydrograph simulations versus parameter sensitivity in a 3-layer TOPMODEL: A case study in a subtropical mountainous watershed, 4th AOGS Annual Meeting, Bangkok, Thailand, 2007.
Krajewski, W. F. and Smith, J. A.: Radar hydrology: rainfall estimation, Adv. Water Resour., 25, 1387–1394, 2002.
Liu, Y. B., Gebremeskel, S., DeSmedt, F., Hoffman, L., and Pfister, L.: A diffusive approach for flow routing in GIS based flood modeling, J. Hydrol., 283, 91–106, 2003.
Nash, J. E. and Sutcliffe, J. V.: River flow forecasting through conceptual models Part 1 – A discussion of principles, J. Hydrol., 10(3), 282–290, 1970.
Singh, V. P.: Effect of spatial and temporal variability in rainfall and watershed characteristics on stream flow hydrograph, Hydrol. Processes, 11, 1649–1669, 1997.
Syed, K. H., Goodrich, D. C., Myers, D., and Sorooshian, S.: Spatial characteristics of thunderstorm rainfall fields and their relation to runoff, J. Hydrol., 271, 1–21, 2003.
Terblanche, D. E., Pegram, G. G. S., and Mittermaier, M. P.: The development of weather radar as a research and operational tool for hydrology in South Africa, J. Hydrol., 241, 3–25, 2001.
Walter, M. T., Steenhuis, T. S., Mehta, V. K., Thongs, D., Zion, M., and Schneiderman, E.: Refined conceptualization of TOPMODEL for shallow subsurface flows, Hydrol. Processes, 16, 2041–2046, 2002.
Wu, R. S., Chen, C. H., and Shih, D. S.: A comparison of gauge and radar-derived rainfall in a land falling typhoon in Taiwan, J. Am. Water Resour. Assoc., 43(2) 281–294, 2007.

Table 1. The rainfall attributes of Matsa and Korsa in Xia-Yun and Xiu-Luan.

Typhoon	Matsa		Korsa	
Watershed	Xia-Yun	Xiu-Luan	Xia-Yun	Xiu-Luan
Total rainfall (mm)	661	881	686	621
Duration (h)	44	47	45	39
RMSE (mm)	6.9	4.6	6.2	4.2
Avg. RI[a] (mm/h)	14.8	18.3	13.7	14.3
Max. RI[b] (mm/h)	39.8	46.8	45.5	41.7

[a] Avg. RI means the average rainfall intensity (total rainfall over duration)
[b] Max. RI is the maximum among hourly rainfall intensities

Table 2. Total rainfall amount in each gauge number class.

Gauge number range	Statistics	Xia-Yun (622 km^2) Matsa	Xia-Yun (622 km^2) Korsa	Xiu-Luan (116 km^2) Matsa	Xiu-Luan (116 km^2) Korsa
2–3	Avg.±Std.	665±146	637±78	841±106	625±40
6–10	Avg.± Std.	670±63	636±31	874±29	623±17
11–19	Avg.± Std.	665±41	642±23	877±13	625±7
24–38	Avg.± Std.	661±18	639±12	879±7	622±4

Avg. is the mean of the 50 sets in each class
Std. is the standard deviation of the class

Table 3. Total discharges in gauge number classes.

Gauge number range	Statistics	Xia-Yun (622 km^2) Matsa	Xia-Yun (622 km^2) Korsa	Xiu-Luan (116 km^2) Matsa	Xiu-Luan (116 km^2) Korsa
2–3	Avg.± Std.	464±122	458±66	519±74	362±26
6–10	Avg.± Std.	468±53	457±26	541±21	361±11
11–19	Avg.± Std.	464±35	462±19	544±9	362±4
24–38	Avg.± Std.	460±15	460±10	545±5	361±2

Table 4. Rainfall and hydrograph RMSEs in gauge number classes among the two watersheds and typhoon cases.

Gauge number range	RMSE	Xia-Yun		Xiu-Luan	
		Matsa	Korsa	Matsa	Korsa
2–3	R Avg.[a]	8.59	7.80	5.45	4.55
	H Avg.[b]	1.75	1.13	0.83	0.33
6–10	R Avg.	6.52	6.19	3.64	3.39
	H Avg.	0.80	0.48	0.24	0.16
11–19	R Avg.	5.45	5.20	2.76	2.59
	H Avg.	0.52	0.35	0.13	0.07
24–38	R Avg.	4.00	3.93	1.91	1.90
	H Avg.	0.23	0.23	0.06	0.03

[a] R Avg. is the average RMSE value of rainfall in the gauge number class
[b] H Avg. is the average RMSE value of hydrograph in the gauge number class

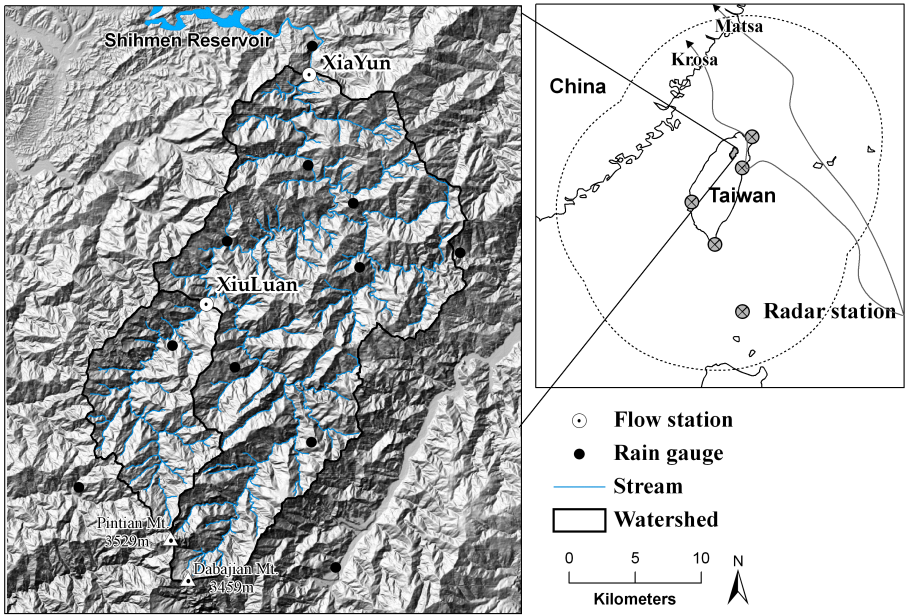

Fig. 1. The location and landscape of study sites. The location and coverage of the four radar stations and the tracks of Matsa and Korsa were shown in the right panel. The topography, raingauges, and flow stations in Xia-Yun and Xiu-Luan watershed were shown in the left panel.

HESSD
5, 2169–2197, 2008

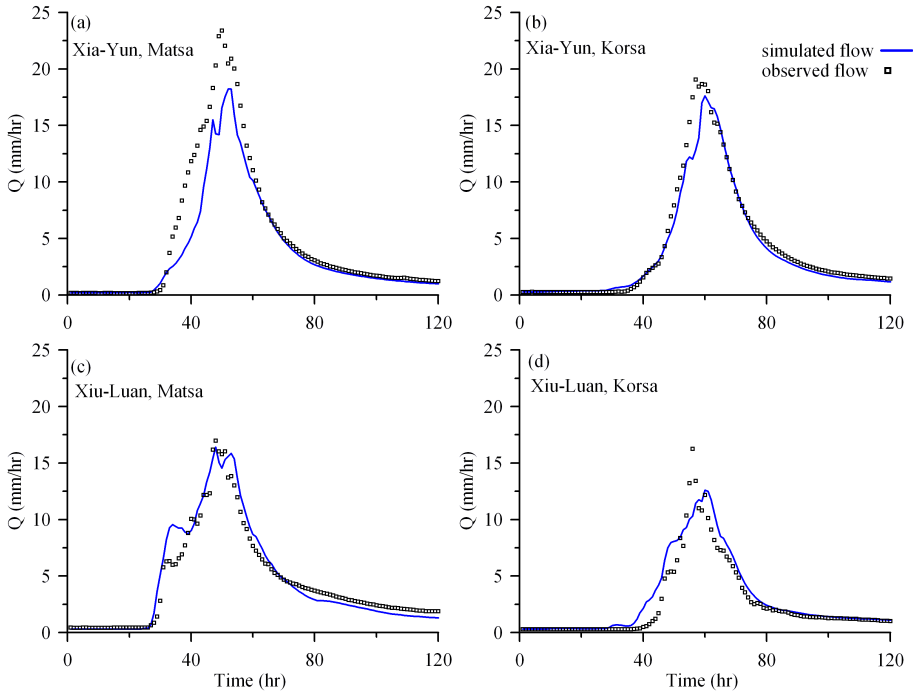

Fig. 2. The observed and simulated hydrographs. The blue lines were simulated flows inputted by radar rainfall and the square indicated the observed flow.

HESSD
5, 2169–2197, 2008

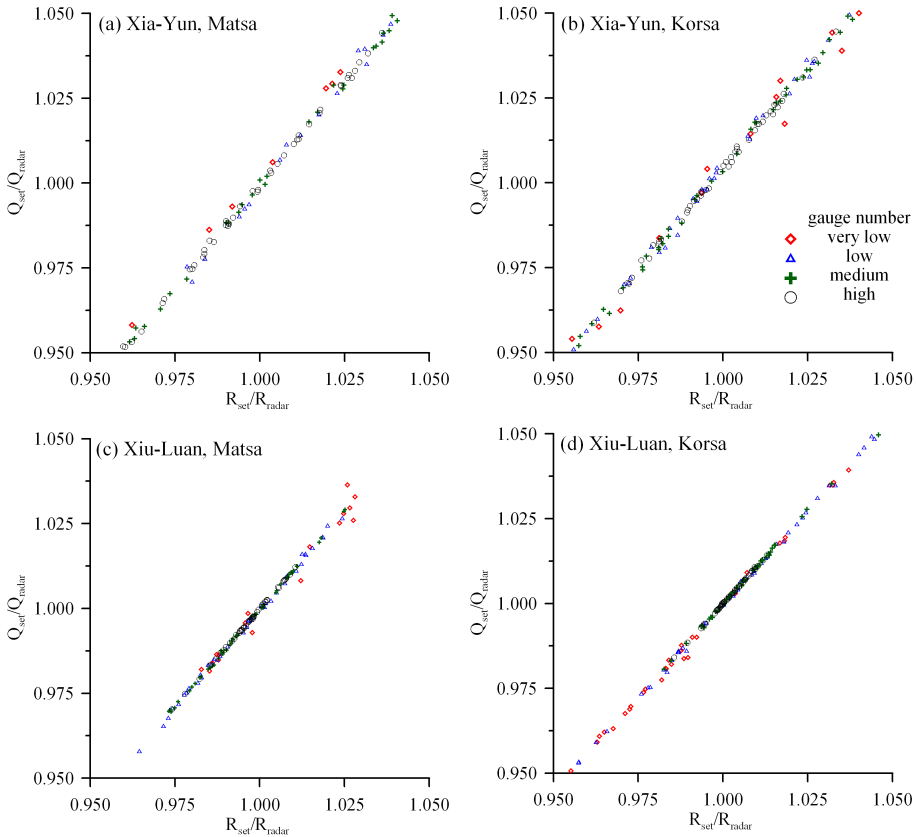

Fig. 3. The scatter plot for discharge amount ratio (Q_{set}/Q_{radar}) and rainfall amount ratio (R_{set}/R_{radar}). The red diamond, blue triangular, green cross and black circle indicated the gauge number of very low, low, medium and high, respectively. **(a)** and **(c)** represented the Matsa case in Xia-Yun and Xiu-Luan; **(b)** and **(d)** represented the Korsa case in Xia-Yun and Xiu-Luan. Some dots outside the axes were not shown.

HESSD
5, 2169–2197, 2008

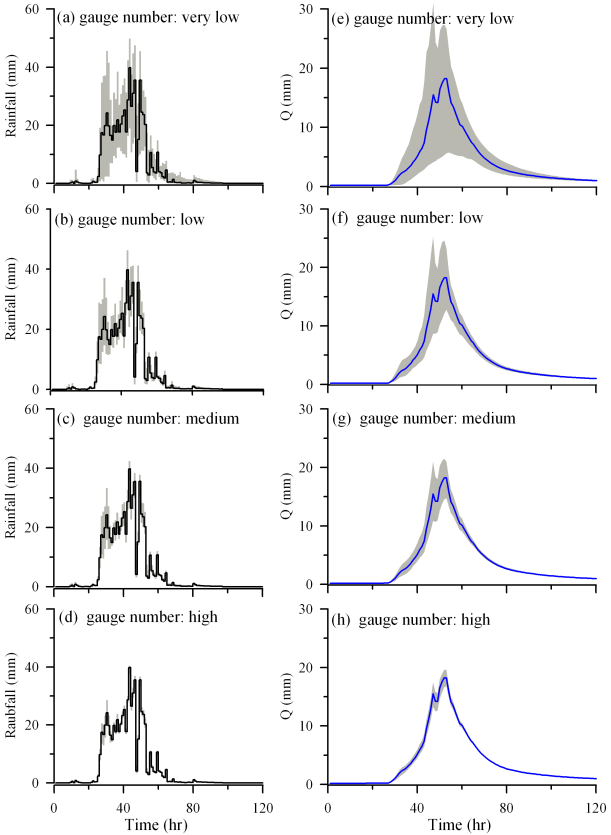

Fig. 4. The hyetographs and hydrographs in Xiayun during Matsa. The hyetograph with solid line was derived from full radar data and the shaded zone in **(a)**, **(b)**, **(c)**, and **(d)** were the ranges among the individual class. The blue solid line was the simulation derived from full radar data and the shaded zone in **(e)**, **(f)**, **(g)**, and **(h)** are the ranges among the individual class.

HESSD
5, 2169–2197, 2008

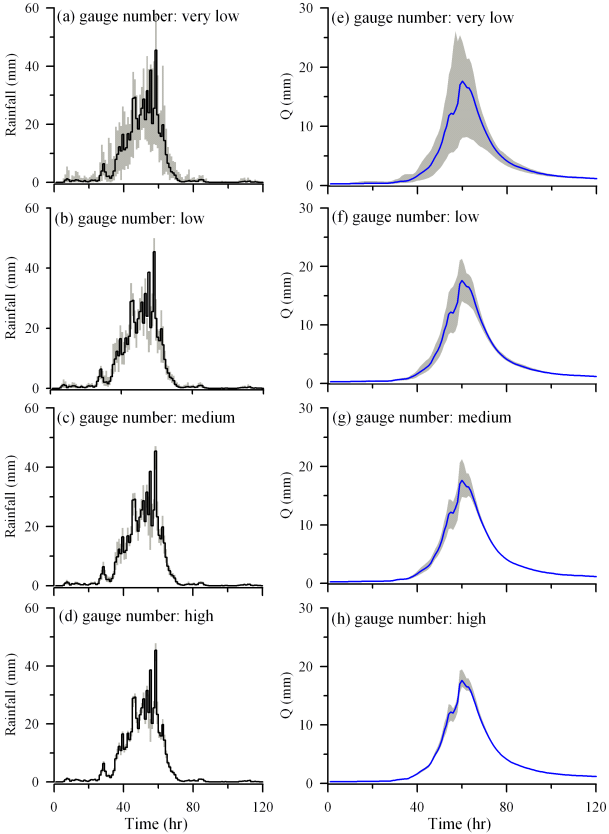

Fig. 5. The hyetographs and hydrographs in Xiuluan during Matsa. The hyetograph with solid line was full radar data and the shaded zone in **(a)**, **(b)**, **(c)**, and **(d)** were the ranges among the individual class. The blue solid line was the simulation derived from full radar data and the shaded zone in **(e)**, **(f)**, **(g)**, and **(h)** were the ranges among the individual class.

HESSD
5, 2169–2197, 2008

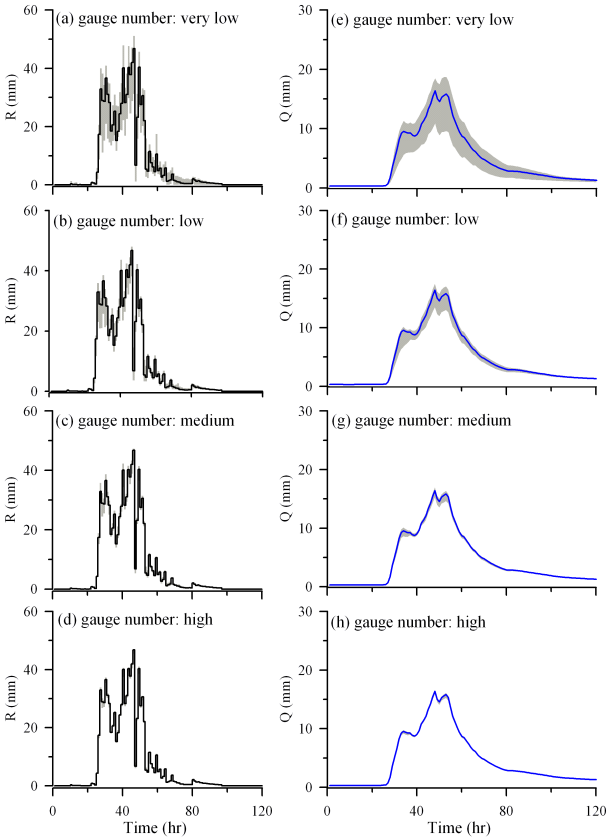

Fig. 6. The hyetographs and hydrographs in Xiayun during Korsa. The hyetograph with solid line was full radar data and the shaded zone in **(a)**, **(b)**, **(c)**, and **(d)** were the ranges among the individual class. The blue solid line was the simulation derived from full radar data and the shaded zone in **(e)**, **(f)**, **(g)**, and **(h)** were the ranges among the individual class.

HESSD
5, 2169–2197, 2008

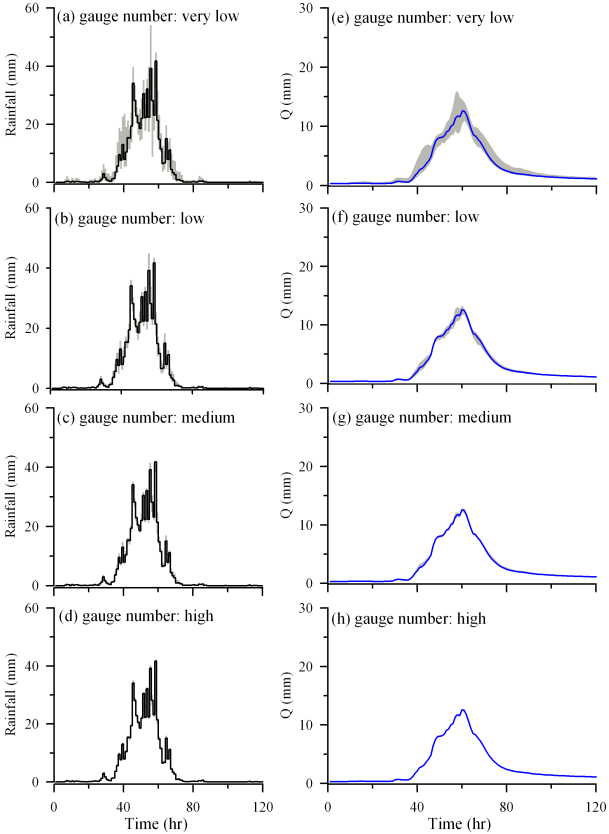

Fig. 7. The hyetographs and hydrographs in Xiuluan during Korsa. The hyetograph with solid line was full radar data and the shaded zone in **(a)**, **(b)**, **(c)**, and **(d)** were the ranges among the individual class. The blue solid line is the simulation derived from full radar data and the shaded zone in **(e)**, **(f)**, **(g)**, and **(h)** are the ranges among the individual class.

HESSD
5, 2169–2197, 2008

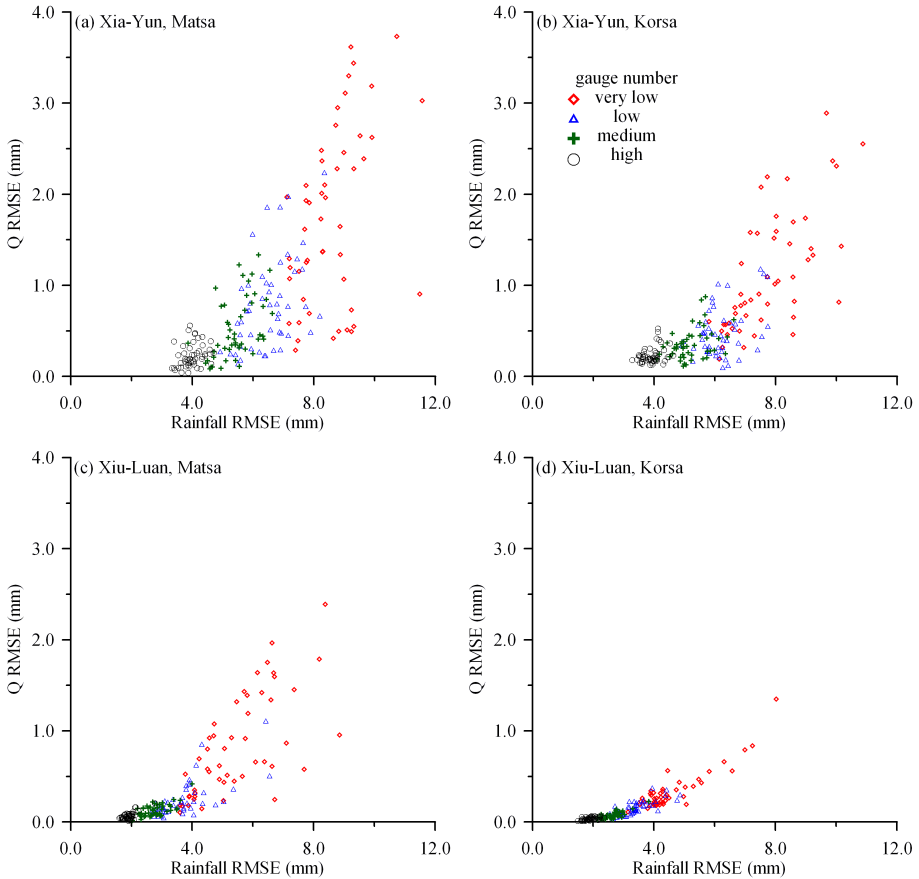

Fig. 8. The scatter plot of Q_{RMSE} and R_{RMSE}. The red diamond, blue triangular, green cross and black circle indicated the gauge number of very low, low, medium and high, respectively. **(a)** and **(c)** represented the Matsa case in Xia-Yun and Xiu-Luan; **(b)** and **(d)** represented the Korsa case in Xia-Yun and Xiu-Luan.

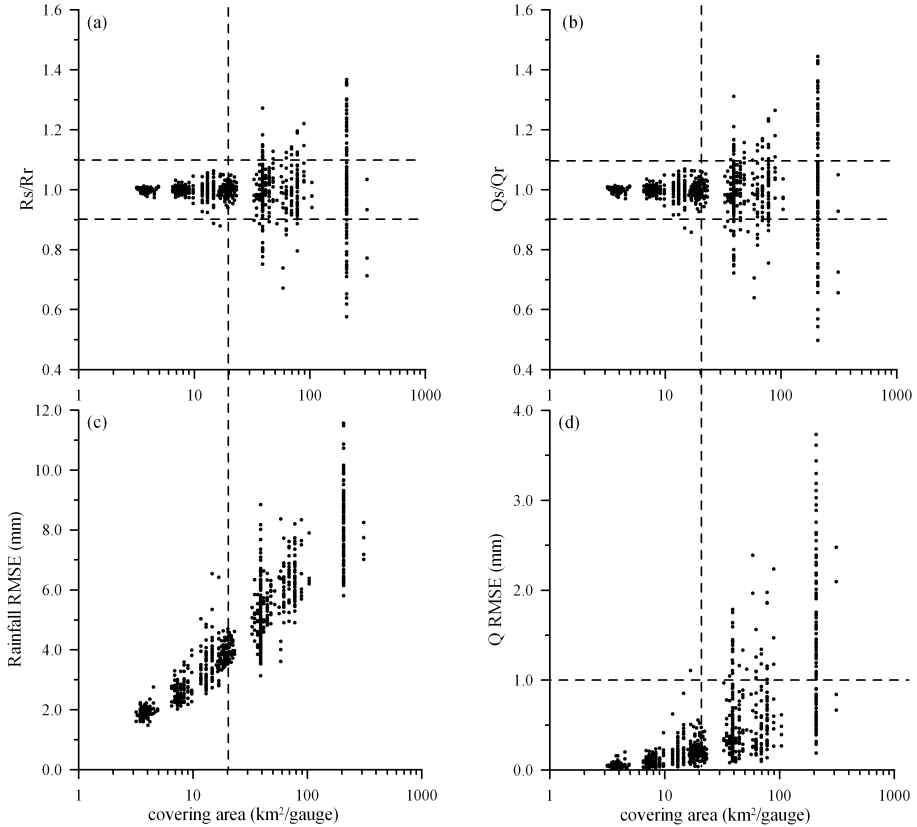

Fig. 9. The relationship between rainfall amount ratio and covering area was presented in **(a)**; the discharge amount ratio and covering area was presented in **(b)**; **(c)** showed the relationship between R_{RMSE} and covering area and **(d)** presented the all cases in Q_{RMSE} and covering area. The horizontal dash lines indicated that amount ration in 0.9 and 1.1, respectively. The vertical dash line is the covering area of 20 km^2/gauge.